phys. stat. sol. (c) **2**, No. 3, 1039–1046 (2005) / **DOI** 10.1002/pssc.200460617

Giant traps associated with extended defects in GaN and SiC

D.C. Look[*1,2], **Z-Q. Fang**[1,2], **A. Krtschil**[3], and **A. Krost**[3]

[1] Semiconductor Research Center, Wright State University, Dayton, OH 45435, USA
[2] Materials and Manufacturing Directorate, Air Force Research Lab., Wright-Patt. AFB, OH 45433, USA
[3] Inst. of Experimental Physics, Otto-von-Guericke-University Magdeburg, 39016 Magdeburg, Germany

Received 9 September 2004, accepted 10 September 2004
Published online 18 February 2005

PACS 61.72.Lk, 61.72.Qq, 71.55.Eq, 71.55.Ht, 72.20.Jv, 73.50.Gr

Extended defects in semiconductors can trap charge and lead to changes in carrier concentration and mobility. Here we consider the trapping effects of pores, microcracks, and dislocations in GaN and SiC, as analyzed by deep level transient spectroscopy (DLTS), transmission electron microscopy (TEM), and scanning surface potential microscopy (SSPM). The defect structures are modeled as spheres, plates, and cylinders for pores, cracks, and dislocations, respectively, and their potentials are directly compared with those measured by holographic TEM and SSPV. The dynamics of the capture and emission processes are investigated by DLTS, although the standard DLTS analysis framework is not applicable here and must be replaced by a more general formalism. As an example, 40-nm-dia. nanopores in SiC can each hold more than 100 electrons, and they exhibit anomalous capture and emission properties.

© 2005 WILEY-VCH Verlag GmbH & Co. KGaA, Weinheim

1 Introduction It is well-known that impurities and point defects can act as donors, acceptors, recombination centers, and traps in semiconductor materials. For simple point charges, models to describe their effects on electrical and optical properties are readily available. Traps, the subject of this paper, are often investigated by deep level transient spectroscopy (DLTS), and the usual analysis of DLTS data is based on the assumption that each trap has a constant capture cross section, independent of time or the presence of nearby traps [1–3]. Thus, if the Fermi level is suddenly raised, say by applying a forward bias to a Schottky contact, electron traps will capture free electrons in an exponential manner, and if the Fermi level is then returned to its original value, the traps will emit the electrons in the same way. However, large defects, such as dislocations, can often hold many charges, and they are not independent of each other [4–8]. In the case of a threading dislocation, the charges can build up along a line, and gradually begin to repel the accumulation of additional charges. Thus, the effective capture cross section decreases as the accumulated fraction becomes larger, and the capture process is no longer exponential with time. The dynamics of dislocation capture were first elucidated in 1989 [5], and since then have been applied to many experimental situations. Recently, it has been shown that pores also can capture charge [7, 8], and that both the capture and emission processes are quite nonexponential [8]. To model this case, a new formalism has been developed [8], and it is applicable to any charge configuration that can be approximated by a sphere, cylinder, or thin slab. Examples of such shapes might include pores, open-core dislocations, and cracks, respectively. In this work, we specifically investigate pores in SiC, and dislocations and microcracks in GaN.

2 Theory Consider a spherical pore of radius r_p with deep, single-level acceptor states of sheet density N_{SS} on its inner surface. If all of the states are filled, then the total number of traps is $4\pi r_p^2 N_{SS}$. However, as more and more electrons are trapped, a negative (repulsive) potential ϕ_{sph} builds up, and the trapping

* Corresponding author: e-mail: David.Look@wpafb.af.mil

© 2005 WILEY-VCH Verlag GmbH & Co. KGaA, Weinheim

rate diminishes. A spherical region depleted of free electrons, described by a local band bending of *energy* $\Phi_{sph} = -e\phi_{sph}(r_p)$, forms outside the surface ($r = r_p$) of the pore. The value of Φ can be calculated from Poisson's equation, which, for spherical pores, is most conveniently expressed in spherical coordinates:

$$\frac{1}{r^2}\frac{d}{dr}r^2\frac{d\phi_{sph}}{dr} = -\frac{\rho}{\varepsilon} = -\frac{eN_D}{\varepsilon} \tag{1}$$

where ρ is the charge density, ε is the static dielectric constant, and N_D is the net donor density (actually, $N_D - N_A$, where N_A is the acceptor concentration). By applying charge conservation and the depletion approximation, it can be shown that the *energy*, $\Phi = -e\phi$, is given by

$$\Phi_{sph}(r,f) = \frac{e^2 N_{SS} r_p f}{\varepsilon}\left\{\frac{N_D}{r_p N_{SS} f}\left[\frac{r^2 - r_p^{\,2}}{6}\right] + \left[1 + \frac{N_D r_p}{3N_{SS} f}\right]\left[\frac{r_p}{r} - 1\right] + 1 + \frac{r_p N_D}{2N_{SS} f}\left[1 - \left(1 + \frac{3N_{SS} f}{r_p N_D}\right)^{2/3}\right]\right\} \tag{2}$$

where f is the fractional occupation of the trap states on the pore, i.e., $f = N_{SS}^-/N_{SS}$. Equation (2) holds for $r_p \le r \le w$, where w is the depletion length, and is cast in a form which is convenient in that the first two terms drop out for $r = r_p$. (For $r \ge w$, $\Phi = 0$.) For our porous SiC sample, $N_D \approx 10^{18}$ cm^{-3} and $r_p \approx 20$ nm, and it will turn out that $N_{SS} \approx 2.5 \times 10^{12}$ cm^{-2}, so that $\Phi(r_p) \approx 0.2$ eV, for f = 1.

For cylindrical pores, it can be shown that

$$\Phi_{cyl}(r,f) = \frac{e^2 N_{SS} r_p f}{2\varepsilon}\left\{\left[1 + \frac{r_p N_D}{2N_{SS} f}\right]\left[\ln\left(1 + \frac{2N_{SS} f}{r_p N_D}\right) - 2\ln\left(\frac{r}{r_p}\right)\right] + \frac{\left(r^2 - r_p^{\,2}\right)N_D}{2r_p N_{SS} f} - 1\right\} \tag{3}$$

for $r_p \le r \le w$. In this case, $\Phi(r_p) \approx 0.3$ eV, for f = 1.

The dynamic capture and emission processes can now be described by the usual master equation:

$$\frac{df}{dt} = -e_n f + c_n(1-f) \tag{4}$$

where e_n is the emission rate from filled traps, and c_n is the capture rate into empty traps. Both rates will be affected (slowed down) by the band bending, as follows:

$$c_n(n,T,f) = \sigma v(T) n e^{-\frac{\Phi_{sph}(r_p,f)}{kT}} \equiv c_{n0}(n,T) e^{-\frac{\Phi_{sph}(r_p,f)}{kT}}\,. \tag{5}$$

$$e_n(T,f) = \sigma_{emis} v(T) N_{CB}(T) e^{-\frac{E_{SS0}+\Phi_{sph}(r_p,f)}{kT}} \equiv e_{n0}(T) e^{-\frac{\Phi_{sph}(r_p,f)}{kT}} \tag{6}$$

where $v(T) = (8kT/\pi m^*)^{1/2}$ is the thermal velocity, $N_{CB}(T) = 2(2\pi m^* kT)^{3/2}/h^3$ is the effective conduction band density of states (in the Boltzmann approximation), n is the free electron concentration, σ is the capture cross section for a single trap, and $\sigma_{emis} = (g_0/g_1)\sigma\exp(\alpha/k)$, where g_0 and g_1 are the degeneracies of the unoccupied and occupied trap states, respectively, and α is a linear temperature coefficient: $E_{SS} = E_{SS0}(1 - \alpha T)$. From Eqns. (4) – (6), a general integral equation, describing both capture and emission, can be written for f(t):

$$\int_{f_\alpha}^{f_\beta} \frac{e^{\frac{\Phi_{sph}(r_p,f)}{kT}}}{1 - f\left[1 + \frac{e_{n0}(T)}{c_{n0}(n,T)}\right]}\,df = c_{n0}(n,T)(t_\beta - t_\alpha) \tag{7}$$

In a DLTS experiment, the capture process is carried out by applying a forward bias to a normally reversed-biased Schottky barrier or p-n junction [1–3]. In reverse bias, the traps are in a region depleted of free electrons, and thus experience a very low free-electron concentration, $n = n_r << n_b$, where n_b is the bulk (neutral) value, 10^{18} cm^{-3} in this case. Thus, $c_{n0}(n_r,T)$ is very small, so that emission dominates and the traps are almost empty. Then, in forward bias, the traps are suddenly exposed to the bulk free-

© 2005 WILEY-VCH Verlag GmbH & Co. KGaA, Weinheim

electron concentration $n = n_b$ for a time t_p, the filling pulse length, and at the end of this pulse the filled fraction is defined as f_p. Thus, the trap *filling* process is described by solving Eq. (7) for f_p under the conditions $f_\alpha = 0$, $f_\beta = f_p$, $n = n_b$, $t_\alpha = 0$, and $t_\beta = t_p$. (One convenient means of solving Eq. (7) is by use of the "root" function in Mathcad [9].)

When the filling pulse has ended at time t_p, i.e., by reapplying the reverse bias, the traps are once again suddenly exposed to a very small value of n, i.e., $n = n_r$. (Note that the solution of Eq. (7) is very insensitive to the exact value of n_r, as long as $n_r << n_b$.) The traps now emit their carriers, so that the original fractional occupation f_p is now reduced to f_e, in total time $t_p + t_e$. Thus, in *emission*, Eq. (7) is solved for f_e under the conditions $f_\alpha = f_p$, $f_\beta = f_e$, $n = n_r$, $t_\alpha = t_p$, and $t_\beta = t_p + t_e$. In the most common form of DLTS methodology, used in commercial instruments and often called the "boxcar" technique [1, 2], the emission curve is evaluated at two points, t_1 and t_2 (referenced to t_p), and the signal strength is measured as $S \equiv f(t_1) - f(t_2)$. Such a signal is simulated simply by solving Eq. (7) at two times, $t_p + t_1$, and $t_p + t_2$.

To illustrate these ideas, we show in Fig. 1 a band profile along a line perpendicular to the sample surface and cutting through a single, spherical pore, of radius 2 nm, and of depth 22 nm (from the surface). Here the Fermi energy E_F in the bulk (depth $z = \infty$) is set at zero, and in this region E_F is very close to the conduction-band energy E_{CB}, at least for this particular sample. While under reverse bias $V_r = -V$, the surface will be held at energy $e(\phi_B - V_r)$, where ϕ_B is the Schottky-barrier potential, and E_{CB} will vary smoothly from $e(\phi_B - V_r)$ at $z = 0$, to $E_{CB} = 0$ at $z \geq w$, the depletion depth. During the filling pulse, it is assumed (in this case) that $E_{CB} = 0$ all the way to the surface (flat-band approximation), although this assumption is not invoked for the actual calculations. The dashed lines in the figure illustrate the potential barrier formed near the surface of a pore due to the captured charge. This barrier begins to build up as soon as the filling pulse is applied, and then recedes when the filling pulse is removed. The changing barrier energy means that the effective capture and emission rates will change continuously with time, as described by Eq. (7).

Before going on, it is instructive to solve Eq. (7) for a particularly simple case, $\Phi(r_p,f) = 0$ (or a constant), which should hold for isolated point charges. The Eq. (7) yields the usual closed-form, exponential solutions for capture and emission:

$$f_{capt}(T,t_p) = \frac{1}{1+\dfrac{e_n(T)}{c_n(n_b,T)}}\left\{1-e^{-[e_n(T)+c_n(n_b,T)]t_p}\right\} \approx \left\{1-e^{-[c_n(n_b,T)]t_p}\right\} \quad (8)$$

$$f_{emm}(T,t) = f_{capt}(T,t_p)e^{-[e_n(T)+c_n(n_r,T)](t-t_p)} \simeq f_{capt}(T,t_p)e^{-e_n(T)(t-t_p)} \quad (9)$$

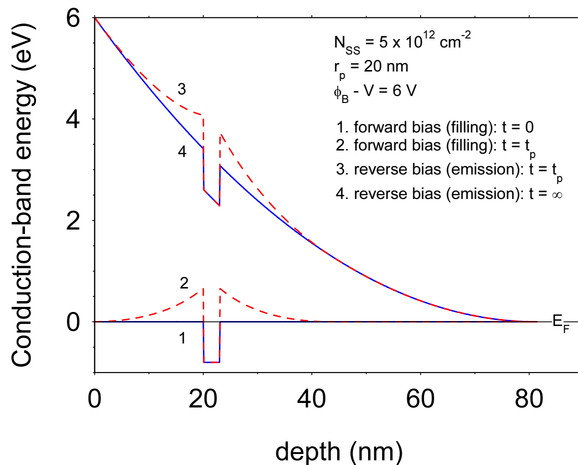

Fig. 1 Conduction band profiles under reverse bias, and forward bias, respectively. The dashed lines denote the bands after the filling pulse (curve 2, at the end of the filling pulse but still in forward bias; and curve 3, immediately after reapplication of the reverse bias).

© 2005 WILEY-VCH Verlag GmbH & Co. KGaA, Weinheim

These equations form the basis of the original DLTS analysis method [1, 2], and are still used in the vast majority of cases, as well as in commercial instruments. Besides isolated point charges, line charges have also been considered in the literature [5, 6], and the derived *capture* process in this case turns out to be logarithmic with time. However, such a time dependence is only an approximation, and to derive it from the general formalism, Eq. (7), we must assume (as did Wosinski[5]) the following: (1) small f, such that the denominator of the integrand in Eq. (7) can be approximated by unity; and (2) $\Phi(r_p,f) \propto f$, which means that the large, bracketed terms in Eqns. (2) or (3), respectively, must be independent of f, i.e., a constant K. Then, Eq. (7) yields a logarithmic solution for f (cf. Eq. (3) of Ref. [6]), which has been seen experimentally for trapping along dislocation lines [5, 6]:

$$f'_{sph}(T,t_p) = \frac{\varepsilon kT}{e^2 N_{SS} r_p K_{sph}} \ln\left[1 + \frac{e^2 N_{SS} r_p K_{sph}}{\varepsilon kT} c_{n0}(n_b,T)t_p\right] \tag{10}$$

where K_{sph} is typically on the order of 0.1 – 1.

3 Pores in SiC The porous SiC in this study was prepared by photo-assisted electrochemical etching [10] of n-type 6H SiC obtained from Sterling Semiconductor Inc. (now part of Dow-Corning Corp.). The electrolyte was a mixture of HF acid and ethanol. The resistivity of the starting material was about 0.2 Ω-cm, and the carrier concentration ~ 10^{18} cm^{-3}. The C-V and DLTS data were obtained by means of a Bio-Rad DL4600 DLTS apparatus, which operated over the temperature range 80 – 450 K. From the C-V data, the carrier concentration in the nonporous SiC was uniform at about 10^{18} cm^{-3}, whereas that in the porous SiC dropped to about 10^{17} cm^{-3} at a depth of about 80 nm. Cross-sectional transmission electron microscopy (TEM), using a 200kV Phillips CM-200 instrument, was used to study the pore size and density. At depths of 50 – 100 nm below the surface, the pore radii ranged in size from 10 – 25 nm, with a density of about 5 x 10^{15} cm^{-3}, increasing with depth. The sizes and densities of these pores are very typical of those found at the same depth (just below the so-called “skin layer”) in other P-SiC samples [7, 10, 11].

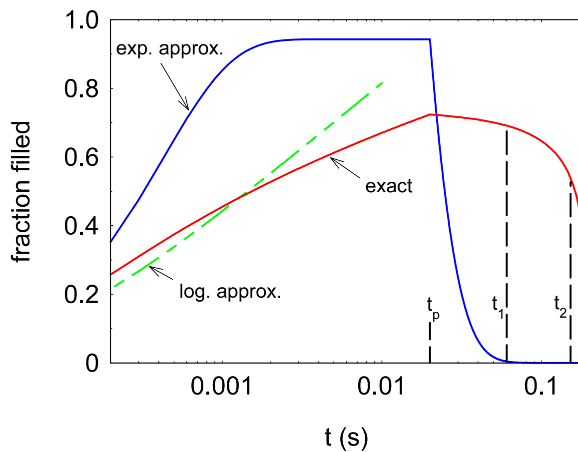

Fig. 2 Fractional occupation, during capture and emission at 350 K, of a pore in porous SiC. An exact calculation is compared with exponential and logarithmic approximations. The filling pulse length is t_p, and the sampling points on the emission transient are t_1 and t_2, respectively.

In Fig. 2, we compare the capture and emission solutions under three different approximations: (1) exact analysis (Eq. (7)); (2) exponential analysis (setting $\Phi_{sph} = 0$, in Eq. (7)); and (3) logarithmic analysis (for f << 1, and $\Phi_{sph} = Ke^2N_{SS}r_pf/\varepsilon$ in Eq. (7)). To generate the curves, we have used some SiC parameters from the literature: $m^*/m_0 = 0.4$, and $\varepsilon/\varepsilon_0 = 10$; some parameters measured by TEM or C-V: r_p = 2 x

© 2005 WILEY-VCH Verlag GmbH & Co. KGaA, Weinheim

10^{-6} cm^{-3}; $N_D \approx n_b \approx 10^{18}$ cm^{-3}; and $n_e \approx 10^9$ cm^{-3} (fit not sensitive to n_e); and some fitted parameters (i.e., those needed to fit the DLTS data of trap T_0 in Fig. 3): $N_{SS} = 2.5 \times 10^{12}$ cm^{-3}; $E_{SS0} = 0.8$ eV; $\sigma = 1 \times 10^{-22}$ cm^2; and $\sigma_{emis} = 3 \times 10^{-13}$ cm^2. A filling pulse length $t_p = 20$ ms was assumed for the curves in Fig. 3. The exponential approximation is the one assumed in the vast majority of DLTS experiments, and indeed, it works well for simple, isolated traps such as T_2 (cf. Fig. 3). However, it rises much too fast to explain the capture process of the pore-type traps (T_0, in Fig. 3). The logarithmic approximation, on the other hand, works fairly well for filling fractions up to about 0.5, but fails beyond that point. From the exact solution, it is seen that even at $t_p = 20$ ms, complete saturation has not taken place. Also, in emission, the exact solution is much slower than the exponential solution, because at higher values of f the emitting electrons experience a strong coulomb barrier and are slowed down. In Fig. 2, we have also simulated a boxcar analysis on the BioRad DL4600 instrument by indicating a common set of sampling points, $t_1 = 61.0$ ms and $t_2 = 152.6$ ms, referenced with respect to t_p. This choice leads to an emission rate of $\ln(t_2/t_1)/(t_2 - t_1) = 10$ s^{-1} at the signal maximum of a trap such as T_2 (Fig. 3), which has an exponential emission (Eqs. 8 and 9). However, the emission for trap T_0 is far from exponential, so that the "standard" analysis will be highly inaccurate in this case.

The experimental DLTS data, for filling pulse lengths of 0.2, 1.0, 5.0, and 20 ms, are shown as dashed lines in Fig. 3. Here we have plotted $\Delta C/C$, where $\Delta C = C(t_1) - C(t_2)$, and C is the equilibrium capacitance under the reverse-bias condition, $V_r = -5$ V. It can be shown that $-\Delta C/C \cong F_\lambda N_T/2N_D$, where N_T is the trap concentration, and F_λ is a factor which is close to unity for small trap concentrations ($N_T << N_D$) and energies that are not too deep, but < 1 otherwise [3]. For our case, $N_T = 4\pi r_p^2 N_{SS} N_p$, where N_p is the volume density of pores. From the TEM measurements, the sheet density of pores is about 3×10^{10} cm^{-2}, and the volume density N_p is then, very approximately, $(3 \times 10^{10})^{3/2} \approx 5 \times 10^{15}$ cm^{-3}. Thus, $N_T \approx 6 \times 10^{17}$ cm^{-3}, and from this value and also $E_T = E_{SS} = 0.8$ eV, we can calculate $F_\lambda = 0.25$ [3]. The actual DLTS signal is $\propto N_T[f(t_1) - f(t_2)]$, as shown in Fig. 2, and $f(t_1) - f(t_2)$ is calculated to be 0.646 at the peak of the 20-ms theoretical curve, in Fig. 3. Thus, from the TEM data, we would predict that $F_\lambda N_T[f(t_1) - f(t_2)]/N_D \approx 0.10$, whereas we actually need a value of about 0.03 to fit the data at the peak, as shown. In other words, we need an N_T value of about 2×10^{17} cm^{-3} to fit the data, which is not outside the error of that determined by TEM (6×10^{17} cm^{-3}), considering that the latter value is a rather crude estimate.

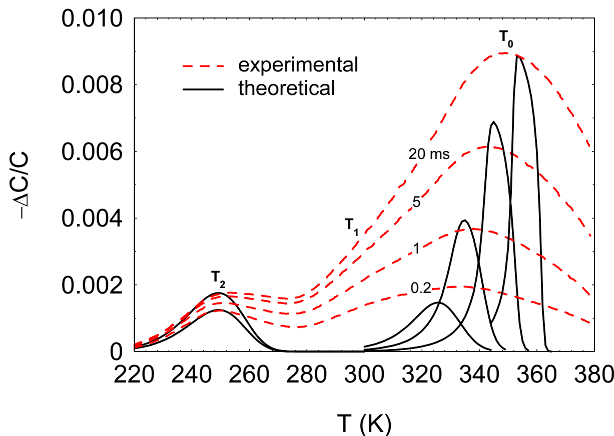

Fig. 3 Experimental (dashed lines) and theoretical (solid lines) DLTS curves for different filling-pulse lengths, 0.2, 2, 5, and 20 ms, in porous SiC. Trap T_2 is a "normal" trap (impurity or point defect), which obeys exponential kinetics, and trap T_0 is related to the pores.

The normalization factor for the 20-ms curve is now applied to the other three theoretical curves, and they reproduce their respective experimental peak magnitudes quite well. Furthermore, the temperature shifts are also well reproduced, giving strong validity to our model. Finally, both the experimental and

© 2005 WILEY-VCH Verlag GmbH & Co. KGaA, Weinheim

theoretical curves become narrower at larger values of t_p. The experimental curves are of course broader than their theoretical counterparts, because we have not considered the known variations in r_p, and the *possible* variations in E_{SS}. The variation in r_p is not likely the cause of the broadening, because neither a doubling nor a halving of the pore size moves the curves by more than a few K. On the other hand, an increase of E_{SS} from 0.80 to 0.85 eV moves the curves up by almost 20 K, which is sufficient to explain the line broadening. Indeed, a ±0.05 eV variation in E_{SS} seems quite reasonable, since some of the pores will undoubtedly be close enough to influence each other. It also should be noted that adding more traps at different values of E_{SS} would also bring the total, fitted N_T closer to the TEM estimate.

4 Microcracks in GaN Freestanding layers of GaN, grown on Al_2O_3 by hydride vapor phase epitaxy and then separated from the Al_2O_3, are beginning to be used as substrates for GaN-based devices. Thus, defects in these layers are of both scientific and practical interest. Because these layers are thick, they are subject to cracking, and this problem must be solved before they can become useful. Recently, we have imaged freestanding GaN with scanning surface potential microscopy (SSPM) [12], and have found features that resemble subsurface microcracks, in that they project onto the surface as a straight, narrow strip, of width about 2 μm. The SSPM image of a 40-μm x 40-μm area is shown in Fig. 4, and a line scan of the potential, in Fig. 5. Note that this potential line scan has a shape much like the energy line scan illustrated in Fig. 1 (except inverted). We can attempt to model the microcrack as a thin, infinite-area box with charge on either side, of sheet density N_{SS}. Since charge balance requires that $N_{SS} = N_D w$, and since $w \approx 2$ μm, from the figure, and $N_D \approx n \approx 6 \times 10^{15}$ cm^{-3}, from Hall-effect measurements, we find that $N_{SS} \approx 1 \times 10^{12}$ cm^{-2}. Then, the potential at the surface should be $\phi \approx eN_{SS}^2/2\varepsilon N_D \approx 16$ V. This value is, of course, much higher than what is actually measured, possibly because the measurement takes place at the "end" of the box, at the surface, and here the potential may be much reduced from the maximum value, say, that toward the middle of the box. Thus, it's difficult to be quantitative in this case, but nevertheless, the line scan shown in Fig. 5 clearly is giving information on the lateral shape of the potential around a crack. To be fully understood, this type of problem will have to be explored in more detail.

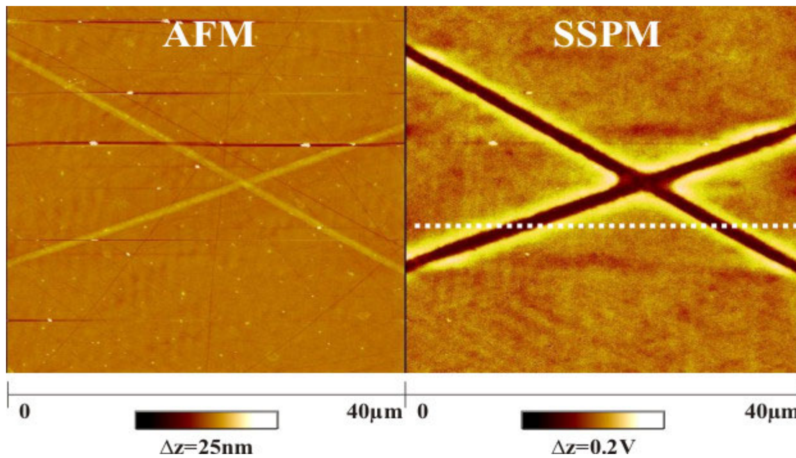

Fig. 4 AFM and SSPM images of microcrack-like defects in HVPE GaN. A line scan of the surface potential, shown in Fig. 5, has a path denoted by the dotted line in this figure.

5 Dislocations in GaN Cherns and coworkers have developed electron holography in conjunction with a transmission electron microscope to study charge on threading dislocations [13, 14]. Basically, the interference fringes in the hologram are affected by an electric field in the vicinity of the sample, and this field is of course directly related to the potential. The potential of a cylindrical charge, given by Eq. (3), is directly applicable to an open-core screw dislocation, of radius r_p, with an acceptor sheet density of N_{SS} on the inner surface. However, to model an *edge* dislocation with this formula, we must imagine a small open core of radius r_p, and then define a line charge as $e2\pi r_p N_{SS} L$, where L is the dislocation length.

© 2005 WILEY-VCH Verlag GmbH & Co. KGaA, Weinheim

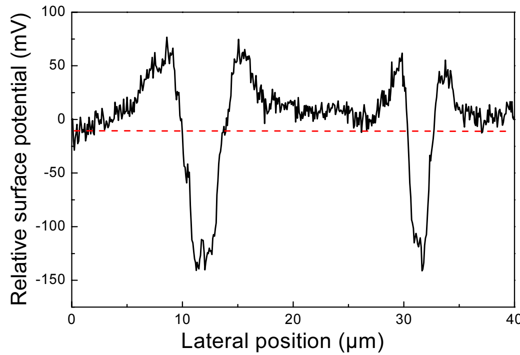

Fig. 5 Lateral profile of the surface potential along the dotted line shown in Fig. 4. Note that the line crosses two cracks.

From end-on images of typical threading-edge dislocations in GaN, it seems that a good value for r_p is about 2 Å. The important parameter for comparison with theory and the results of other experiments is the charge per unit length, $e2\pi r_p N_{SS}$. Even more conveniently, it can be normalized to the c-axis parameter, as $e2\pi r_p N_{SS}c$, where c = 5.185 Å. Cherns' data (Fig. 3 of Ref. [14]) are presented in Fig. 6, and our fit of these data is also shown. For this sample, $N_D \sim 10^{17}$ cm^{-3}, and the best fit of the potential is then found for $N_{SS} \sim 2.6 \times 10^{14}$ cm^{-2}, giving a normalized line charge $e2\pi r_p N_{SS}c$ = 1.7 e per c-lattice distance (e/c). Cherns also attempted a fit, but with a much simpler model of the potential, neglecting screening. Nevertheless, his fitted line charge was about 2e/c, not much different than ours. It should also be mentioned

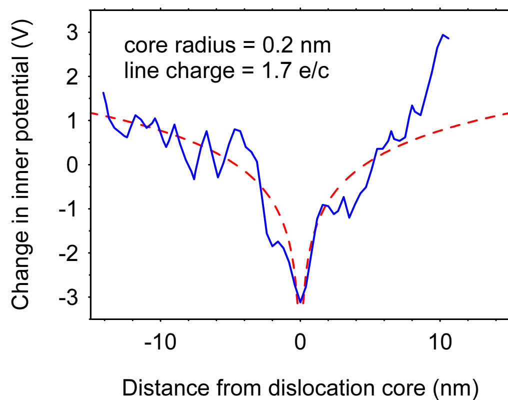

Fig. 6 Lateral potential profile across a threading-edge dislocation in GaN. The dotted line is a theoretical fit, assuming a line charge of 1.7 e/c.

that we have added a positive background potential of 2.6 V in order to fit the data more accurately. It would be interesting to apply a pulsed external potential to this dislocation and study the dynamics of carrier trapping and emission, as was done for the pores in SiC, considered earlier.

6 Summary Many types of extended defects, including dislocations, pores, and cracks, can trap multiple charges. The capture and emission kinetics of these large traps vary with the amount of charge, and thus cannot be described by closed-form exponential formulas, except at very small filling fractions. At somewhat larger filling fractions, the capture process can have a logarithmic time dependence; however, usually, a numerical solution is required. The general model requires knowledge of the potential around the defect, and indeed, the potentials around dislocations and cracks in GaN have been directly deter-

© 2005 WILEY-VCH Verlag GmbH & Co. KGaA, Weinheim

mined by holographic TEM and SSPM, respectively. However, in these cases, the trapping *kinetics* have not yet been studied. In porous SiC, the potential around a spherical pore has been calculated (although not directly measured), and this result has been successfully used to reproduce the experimental DLTS signals (capture and emission kinetics) associated with the pores.

Acknowledgements We wish to thank T.A. Cooper, J.E. Hoelscher, and W. Rice for technical assistance, and B. Claflin, G. Farlow, and P.W. Yu for helpful discussions. DCL and ZQF were supported by ONR Grants N00014-01-1-0715 and N00014-03-1-0467 (monitored by C. Wood), AFOSR Grant 49620-03-1-0197 (G. Witt), and Air Force Contract F33516-00-C-5402 (J. Brown).

References

[1] D. V. Lang, J. Appl. Phys. **45**, 3023 (1974).
[2] D. C. Look, Electrical Characterization of GaAs Materials and Devices (Wiley, New York, 1989).
[3] D. C. Look and J. R. Sizelove, J. Appl. Phys. **78**, 2848 (1995).
[4] T. Figielski, Solid-State Electron. **21**, 1403 (1978).
[5] T. Wosinski, J. Appl., Phys. **65**, 1566 (1989).
[6] A. Hierro, A. R. Arehart, B. Heying, M. Hansen, J. S. Speck, U. K. Mishra, S. P. DenBaars, and S. A. Ringel, phys. stat. sol. (b) **228**, 309 (2001).
[7] P. A. Ivanov, M. Mynbaeva and S. E. Saddow, Semicond. Sci. Technol. **19**, 319 (2003).
[8] D. C. Look, Z-Q. Fang, S. Soloviev, T. S. Sudarshan, and J. J. Boeckl, Phys. Rev. B **69**, 195205 (2004).
[9] Mathsoft, 101 W. Main St., Cambridge, MA 02142.
[10] S. Soloviev, T. Das, and T. S. Sudarshan, Electrochem. Solid State Lett. **6**, G22 (2003).
[11] A. Sagar, C. D. Lee, R. M. Feenstra, C. K. Inoki, and T. S. Kuan, J. Appl. Phys. **92**, 4070 (2002).
[12] A. Krtschil, A. Dadgar, and A. Krost, J. Cryst. Growth **248**, 529 (2003).
[13] D. Cherns and C. G. Jiao, Phys. Rev. Lett. **87**, 5504 (2001).
[14] D. Cherns, C. G. Jiao, H. Mokhtari, J. Cai, and F. A. Ponce, phys. stat. sol. (b) **234**, 924 (2002).

© 2005 WILEY-VCH Verlag GmbH & Co. KGaA, Weinheim